Journal of Hazardous Materials 165 (2009) 240–249

Contents lists available at ScienceDirect

Journal of Hazardous Materials

journal homepage: www.elsevier.com/locate/jhazmat

Preparation and characterisation of raw chars and physically activated carbons derived from marine *Posidonia oceanica* (L.) fibres

M.C. Ncibi[a,b,c,*], V. Jeanne-Rose[c], B. Mahjoub[a,b], C. Jean-Marius[c], J. Lambert[d], J.J. Ehrhardt[d], Y. Bercion[e], M. Seffen[a,b], S. Gaspard[c]

[a] *Laboratoire de chimie, Institut Supérieur Agronomique, Chott Meriem 4042, Sousse, Tunisia*
[b] *Unité de Recherche "Chimie Appliquée et Environnement", EPAM Sousse 4000, Tunisia*
[c] *Laboratoire COVACHIMM, EA 3592 Université des Antilles et de la Guyane, BP 250, 97157 Pointe à Pitre Cedex, Guadeloupe, France*
[d] *Laboratoire de Chimie Physique et Microbiologie pour l'Environnement, UMR 7564 CNRS, Universités de Nancy, 405, rue de Vandœuvre, F 56600 Villers-lès-Nancy cedex, France*
[e] *Groupe de Technologie des Surfaces et Interfaces (GTSI), EA 2432, Faculté des Sciences Exactes et Naturelles, Université des Antilles et de la Guyane, BP 250, 97157 Pointe à Pitre Cedex, Guadeloupe, France*

ARTICLE INFO

Article history:
Received 7 March 2008
Received in revised form
26 September 2008
Accepted 29 September 2008
Available online 15 October 2008

Keywords:
Posidonia fibres
Char
Physical activation
Adsorption
Modelling

ABSTRACT

Industrial valorisation of low cost and renewable biomass as raw precursor of activated carbon for environmental applications is an interesting alternative to costly commercial activated carbons. In this study, the possible use of Mediterranean, *Posidonia oceanica* fibrous biomass, as a precursor for chars and physically activated carbons, is investigated. Firstly, the raw marine material was chemically and biochemically characterised throughout dry-basis elemental, X-ray photoelectron spectroscopy (XPS) and scanning electron microscopy (SEM) analysis. Then, several *P. oceanica* chars were prepared and characterised under different pyrolysis times and temperatures. In addition, physically activated carbons (PACs) were produced via water steam flow under various activation periods.

The results showed that the pyrolysis induces the creation of pores at different levels with respect to the involved temperature. Thereafter, the physical activation tends to enhance the development of the porous structure. In that issue, the performed Brunauer–Emmett–Teller (BET) and Barrett–Joiner–Halenda (BJH) analysis revealed that the prepared PACs have a mainly mesoporous inner morphology with a varying fraction of micropores.

1. Introduction

Adsorption techniques have gained favour in recent years because of their proven efficiency in industrial purification of both liquid and gaseous media, and chemical recovery operations. In that issue, the most extensively used sorbents are definitely activated carbons (ACs). In general, they are particularly advantageous because of their high internal surface areas (typically in the range of 500–2500 m^2/g) and functionalised surfaces (generally acido–basic sites). Indeed, adsorption characteristics of activated carbon are mainly determined by its porous structure (magnitude and distribution of pore volume) and surface chemistry (due to heteroatomic functional groups), which make AC very versatile sorbent-materials.

Nevertheless, the properties and suitability of activated carbons towards specific applications is dictated in large measure by the precise character of the porosity of the carbon. In particular, the size, shape and the distribution of pores, as well as their surface chemistry heavily influence the characteristics of the porous material and its suitability for a given application [1–3].

Basically, ACs use to be produced from natural materials such as wood, peat lignite and bones, which would increase the overall production cost. Recently, many alternative biological materials with low or null cost have been used as precursors in the production process of activated carbons including cottons stalks [4], agricultural by-products [5], *Eucalyptus* [6], date pits [7], fruits stones and shells [8] and bamboo [9].

When using AC, the adsorption process results from interactions between the carbon surface and the adsorbate. These interactions can be electrostatic or non-electrostatic. When the adsorbate is an electrolyte that dissociates in aqueous solution, electrostatic interactions occur; the nature of these interactions, that can be attractive or repulsive, depends on the: (i) charge density of the carbon surface; (ii) chemical characteristics of the adsorbate; and (iii) ionic

* Corresponding author at: Laboratoire de chimie, Institut Supérieur Agronomique, Chott Meriem 4042, Sousse, Tunisia. Tel.: +216 73348546 fax: +216 73348691.
E-mail address: ncibi_mc@yahoo.com (M.C. Ncibi).

0304-3894/$ – see front matter © 2008 Elsevier B.V. All rights reserved.
doi:10.1016/j.jhazmat.2008.09.126

strength of the solution. Non-electrostatic interactions are always attractive and can include: (i) van der Waals forces; (ii) hydrophobic interactions; and (iii) hydrogen bonding.

Activation can be accomplished by one of two distinct processes: (i) chemical activation or (ii) physical activation. The porosity of chemically activated products is generally created by dehydration reactions occurring at significantly low temperatures with chemical agents such as phosphoric acid, potassium hydroxide, zinc chloride, etc. The fabrication of activated carbon produced by physical activation involves two main steps: carbonisation of the raw material in absence of oxygen, and activation of the carbonised product with water vapour, carbon dioxide or air (the air being carefully introduced in the reactor in order to prevent carbon–oxygen gasification [10]).

To our knowledge, *Posidonia oceanica* (L.) fibres balls were not studied so far as activated carbon precursor. Thus, in this research, we attempt to valorise such renewable, low cost, easily available and highly abundant marine biomass in producing raw char (pyrolysis only) and physically activated carbons PACs (pyrolysis and steam activation). The effect of some treatments (heating time and temperature) will be investigated, as well as an exhaustive textural and chemical characterisation of the produced carbonaceous material (char and PACs).

2. Materials and methods

2.1. Precursor preparation and characterisation

P. oceanica leaf sheaths (basal parts of leaves of the Mediterranean seagrass) were collected from Chott-Meriem bay (Sousse, Tunisia). The fibres are manually separated, washed thoroughly with distilled water to remove salt and then dried in an oven at 40 °C for 48 h to a constant weight. After drying, the fibres were immediately stored in desiccators.

Then, an elemental (C, H, O, N, K, P, Ca, Na, Fe) content were determined using a Carlo Erba 1106 Elemental Analyzer. Furthermore, the estimation of the biochemical content (i.e. cellulose, hemicellulose, lignin and extractives), as well as the textural characterisation (scanning electron microscopy) were also carried out. The biochemical composition was determined by performing standards analyses for lignin (Klason lignin), pentosan (as hemicellulose) and cellulose (Kurssher and Hoffer method), for which the technical procedures has been previously described [11]. The ash content was estimated by heating the sample at 550 °C in a muffle furnace for 2 h in the presence of air and until no mass variation was observed [12]. The moisture content was calculated by weight difference employing a muffle oven and heating the sample (2 g) at 105 °C until the dried matter become constant [12].

2.2. Thermogravimetric analysis

The experiments were performed using a Setaram France TG-DSC 111, G11 instrument. 8.76 mg of the Posidonia sample is heated in a thermobalance from 25 to 700 °C at a heating rate of 10 °C/min, under an argon flow of 80 mL/min.

2.3. Char fabrication

Preparation of chars from raw *P. oceanica* fibres was carried out by carbonising an acutely weighted amount of the marine biomass. Pyrolysis consisted of slow heating in a horizontal quartz tube and inserted into a horizontal furnace (Thermolyne F 21100) under a nitrogen flow of 80 mL/min. The biomass sample was placed on a support in the middle of the hot zone of the reactor and heated at a controlled heating rate of 10 °C/min to the final temperature and held at that temperature for 1 and 2 h, respectively. Different carbonisation temperatures were investigated (300, 400, 500, 600, 700 and 800 °C). Once finished, the residual char was removed from the reactor and weighed to estimate the weight loss of the sample (i.e. difference in weight before and after pyrolysis).

2.4. Physical activation protocol

The approach used in this study to fabricate PACs is the simultaneous pyrolysis-activation process. Thus, the biomass was pyrolysed as mentioned in the previous section under 600 °C of temperature and 1 h of heat exposure (i.e. those operating conditions lead to an average weight loss of about 62%). Thereafter, the char derived from the pyrolysis step was activated in the same reactor at a water steam flow rate of 80 mL/min. The sample was heated at 10 °C/min to the final temperature of 600 °C. Then, the resulting materials were washed with water in a Soxhlet extractor. The effect of activation time was investigated in this research for values between 20 and 720 min. The burn-off or degree of carbon loss was calculated as follows:

$$\text{Burn-off} = \frac{(w_1 - w_2)}{w_1} \times 100 \ (\%) \quad (1)$$

where w_1 is the initial dry char weight (g) and w_2 the mass of char after activation (g).

2.5. Chemical and textural characterisation

Adsorption characterisation for chars and PACs produced from *P. oceanica* at different pyrolysis and activation times was determined via nitrogen adsorption at 77 K and a relative pressure (P/P_0) range of 0.001–1 using a Coulter SA3100 sorptiometer. The Brunauer–Emmett–Teller (BET) total surface area was calculated from the adsorption isotherms using the BET equation where monolayer coverage of nitrogen molecules is assumed to be complete. To conduct calculations using the BET model, it was assumed that the surface area, S_{BET}, is related to the monolayer capacity by the Eq. (2).

$$S_{BET} = \left(\frac{n_m}{22400}\right) a_m L \quad (\mathrm{m^2/g}) \quad (2)$$

where n_m is the monolayer capacity of the solid, defined as the amount of adsorbate which can be accommodated in a completely filled, single molecular layer on the surface of unit mass (1 g) of the solid (mg/g), 22,400 (mL) is the occupied volume of a mol of N_2 at STP (i.e. standard temperature and pressure), a_m is the average surface occupied by a molecule of the N_2 in the completed monolayer (16.2×10^{-20} m^2) and L is the Avogadro constant (6.023×10^{23} molecules). The pore size distribution was estimated using the Barrett–Joiner–Halenda (BJH) equation during the desorption phase [13]. In that issue, the BJH method is based on the Kelvin equation, which relates the relative pressure of nitrogen in equilibrium with the porous solid to the size of the pores where capillary condensation takes place. The pore size radii covered by the BJH calculations ranged from 17 to 3000 Å [14].

Besides, the surface properties of the ACs were measured by XPS (X-ray photoelectron spectroscopy). XPS measurements were conducted on an Axis-Ultra DLD Model from KRATOS, equipped with a hemispherical electron analyzer and a monochromatised Al-K (1486.6 eV) X-ray exciting source. Thanks to the high sensitivity of the DLD detector a source power of 90 W was enough to obtain high quality spectra in a reasonable acquisition time. The XPS allows identification and quantification of the elements and the functional groups on the surface of ACs. As the samples were conducting materials, no charge correction was applied to the spec-

tra. The instrument work function was calibrated to give a binding energy (BE) of 83.96 eV for the Au 4f7/2 line for metallic gold and the spectrometer dispersion was adjusted to give a BE of 932.62 eV for Cu 2p3/2 line for metallic copper.

In addition, a scanning electron microscope (SEM) equipped with an energy dispersive X-ray microanalysis (Hitachi S-2500) was used to determine the surface textural characteristics and elemental composition of the experimented sorbents. The chars and PACs were firstly mounted on an aluminium stub, and for the case of the raw posidonia, the fibres were covered with a thin layer of carbon. Then, the microscope was operated at an accelerating voltage of 200 kV and a working distance of 35 mm.

3. Results and discussions

3.1. Raw precursor characterisation

The elemental, ash and moisture content analysis of dry *P. oceanica* fibres, as well as the estimation of the biochemical content (i.e. cellulose, hemicellulose, lignin and extractives) are illustrated in Table 1. The contents of carbon, hydrogen and oxygen were similar to those previously reported in case of other lignocellulosic materials such as vetiver roots [3], cherry stones [15] and olive seed [16], which have a content of C = 46–49%, H = 5.7–6% and O = 39–46%.

Dealing with the biochemical composition, it was shown in Table 1 that holocellulose (cellulose + hemicellulose) constitutes the major component at 59%, and the content of extractives and ash are 12.2 and 1.8%, respectively. Besides, having a quite high lignin content (about 27%), *P. oceanica* fibres could already be considered as a promising biological precursor for activated carbon production [17].

Furthermore, the textural characterisation of the *P. oceanica* fibres was carried out via the SEM technique. Thus, external and transversal observations (Fig. 1A and B, respectively) were carried out on the *P. oceanica* fibres to have an idea on the precursor itself and, thereafter, to figure out the structural changes occurring on this biomass once pyrolysis and activation are performed. Basically, the main observation is that the raw biomass has a typical compact lignocellulosic fibrous structure. Besides, the transversal section (Fig. 1B) shows that intrinsically raw *P. oceanica* is not porous. Indeed, like all lignocellulosic-based fibres, the posidonia ones are formed by several holocellulosic microfibres, which are linked together via lignin.

Table 1
Elemental analysis, biochemical content, ash and moisture of raw *P. oceanica* fibres (wt.%, dry basis).

	Content (% dry basis)
Biochemical composition	
Cellulose	38
Hemicellulose	21
Lignin	27
Extractives	12.2
Elemental analysis	
Carbon	42.10
Oxygen	34.66
Hydrogen	6.44
Sodium	0.49
Calcium	2.48
Potassium	0.48
Sulfur	3.78
Nitrogen	1.52
Magnesium	1.12
Phosphorus	0.05
Iron	97.8 ppm
Magnesium	195.2 ppm
Manganese	34.9 ppm
Zinc	8.8 ppm
Ash	1.8%
Moisture	16%

On the other hand, the XPS analysis (Fig. 2) of raw *P. oceanica* fibres illustrates that for the marine precursor, the carbon content C1s is 42.10% and the oxygen O1s 34.66%, which agrees the previously realised elemental analysis (*cf.* Table 1). For the coming experiments, the XPS deduced O/C ratio would be an interesting factor to investigate, mainly in order to monitor the carbonisation process. The reference O/C ratio for this study (i.e. related to raw fibre) is about 0.82.

3.2. Thermogravimetric behaviour

The thermogravimetric (TG) and differential thermogravimetric (DTG) curves are presented Fig. 3. The (DTG) curve shows

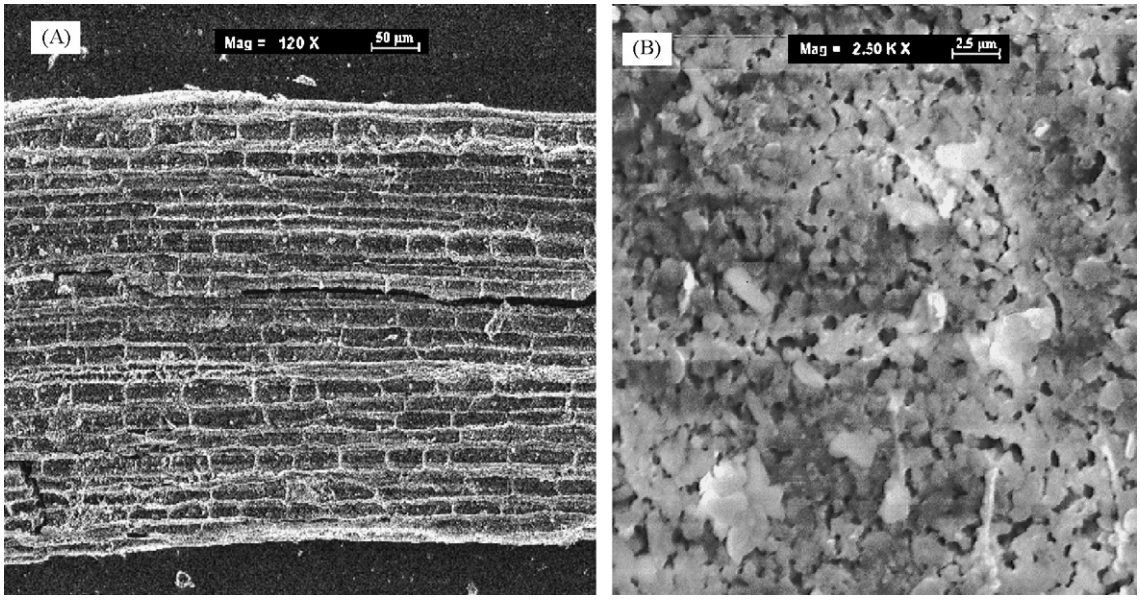

Fig. 1. SEM images of raw *P. oceanica* fibres: external (A) and transversal section (B) micrographs.

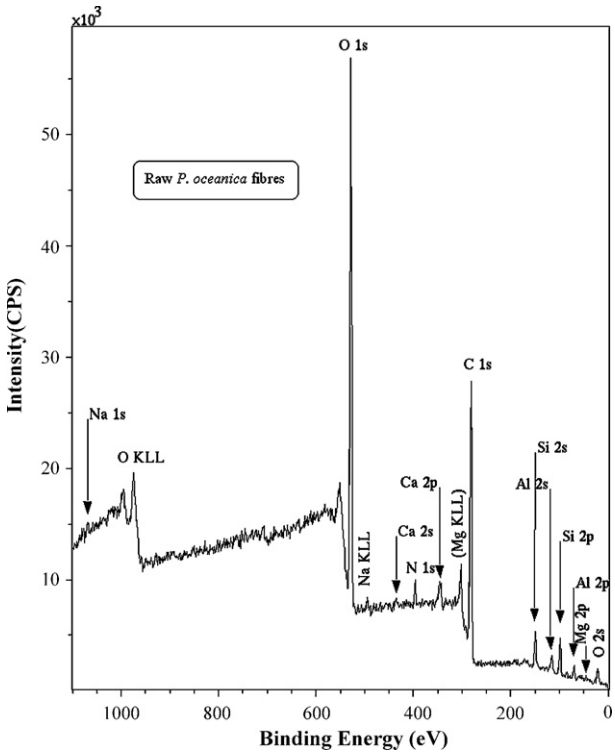

Fig. 2. XPS spectrum of raw *P. oceanica* fibres.

four peaks: the first one with a minimum around 80 °C, corresponding to a mass loss (9.5%) that may be due to water desorption, as previously proposed [18–20], with an endothermic effect (ΔH = 197.28 J/g).

The DTG curve exhibits a second peak around 290 °C, a third one around 330 °C and a last peak around 405 °C. In accordance with several authors proposal, this second peak around 290 °C may correspond to hemicellulose, with a weight loss of 11.5% (initially representing 21% in the *Posidonia oceanica* (L.) fibres). For comparison, the peak corresponding to the weight loss of hemicellulose is located at 340 °C for sugar cane bagasse as described by Várhegyi et al. [21] and at 300 °C for olive stones [22]. The third peak would correspond to the degradation of the cellulose (loss weight of 24.9%). This component representing 38% of the weight of the fibre shows the greater weight loss around 330 °C. Higher but similar temperature values were found for the degradation temperature of cellulose in sugar cane bagasse (395 °C) and olive stones (380 °C) as reported by Várhegyi et al. [21] and Caballero et al. [22], respectively.

The last peak corresponds to lignin degradation occurring at 400 °C similarly to the findings of the aforementioned authors. The weight loss value of lignin is 9.7% for *Posidonia*. The degradation

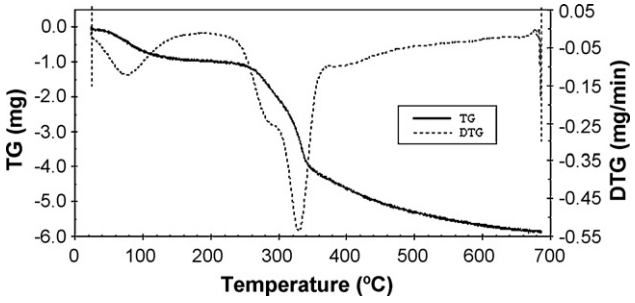

Fig. 3. TG and DTG curves of *P. oceanica* fibres in argon atmosphere.

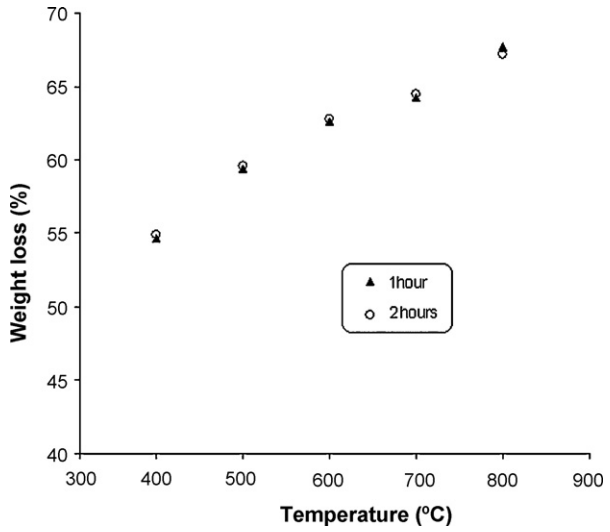

Fig. 4. Effect of pyrolysis temperature on the weight loss of the produced chars.

of the three component, cellulose, hemicellulose and lignin, occur with an exothermic effect with the corresponding enthalpy values, ΔH, −24.63 J/g, −31.91 J/g and −11.41 J/g, respectively.

Nevertheless, above 500 °C, no significant weight loss is observed, indicating that a temperature of 600 °C could be chosen for preparation of the chars.

3.3. Pyrolysed chars

3.3.1. Effect of heating time and temperature

Several heating temperatures have been experimented in the pyrolysis process of raw *P. oceanica* fibres, as well as to heating period (1 and 2 h). As shown in Fig. 4, the increase in the pyrolysis temperature was proportional to an increase in the weight loss. Indeed, from a temperature of 400–800 °C, the biomaterial loss in weight passed from 54.6 to 67.7%, for a heating exposure of 1 h. The increase in temperature quickens the volatilisation reactions of the amorphous components which obstruct the pores. Also, the temperature increase would enhance the gaseous release of carbon monoxide and water within the marine biomass. Such tendency was previously mentioned by others researchers [17,23].

Dealing with the two heating times (1 and 2 h), no statistically significant difference was depicted between the weight losses for all produced chars. For instance, for a temperature of 500 °C, the weight loss was 59.4% for 1 h and 59.6 for 2 h (Fig. 4), which means an error deviation less than 1% (3‰). However, a deeper investigation has to be realised on that issue to find out the effect of increasing the heating time on both chemical and textural composition of the produced chars.

3.3.2. Porosity and surface area

The adsorption capacity of carbonaceous matrices can be identified from their textural and physical characteristics including porosity, surface area and pore size. Fig. 5 depicts the isotherm of nitrogen adsorption at 77 °K for a sample of *P. oceanica* derived char (pyrolysis at 600 °C for 1 h) and Fig. 6A the pore size distribution of the same sample. Basically, the low N_2 adsorbed volume at P/P_0 equal to unity (50.2 cm^3/g) indicated that the pyrolysis phase, under the used operation conditions, was not able to induce the creation of a microporous structure. Such assumption will analytically be confirmed by studying the isotherm shape with respect to the BDDT (Brunauer–Deming–Deming–Teller) classification of

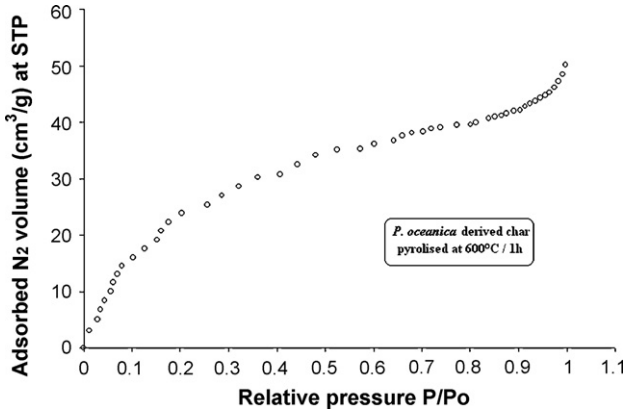

Fig. 5. Adsorption isotherm of nitrogen at 77 °K by *P. oceanica* derived char pyrolysed at 600 °C for 1 h.

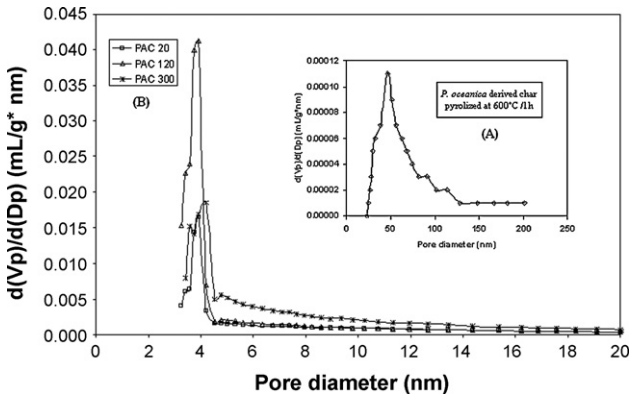

Fig. 6. BJH pore size distribution of a *P. oceanica* char sample (A) and some PACs samples (B).

isotherms [24] and carrying out some calculations on the desorption phase, according to the BJH itinerary.

Hence, as shown on Table 2, the produced char provides a quite low BET surface (111 m^2/g) and has essentially a mesoporous structure Indeed, 80% of its total pores are mesopores with pore width comprised between 2 and 50 nm (i.e. a mesoporous volume equal to 0.028 cm^3/g, from a total porous volume of about 0.035 cm^3/g). The micropore proportion in that case is 11% of the total created pores.

On the other hand, compared to the standard BDDT isotherm classification, the shape of the isotherm may be included in the type II, with a obvious increase of N_2 amount retained at both very low values of P/P_0 (<0.2) and higher relative pressure ($0.8 < P/P_0 < 1$). Thus, the *P. oceanica* char was revealed to possess a low value

Table 2
Surface and porous texture parameters of *P. oceanica* derived char (pyrolysed at 600 °C for 1 h).

	P. oceanica derived char
BET surface area (m^2/g)	111
Total surface area (m^2/g)	110
t-Plot external area (m^2/g)	141
Total pore volume (cm^3/g)	0.035
Micropore volume (cm^3/g) ($d < 2$ nm)	0.004 (11%)[a]
Mesopore volume (cm^3/g) (2 nm < d < 50 nm)	0.028 (80%)[a]
BJH average pore width (nm)	16.99
Bulk density (g/cm^3)	0.594

[a] Porosity percentage; *d*: pore diameter.

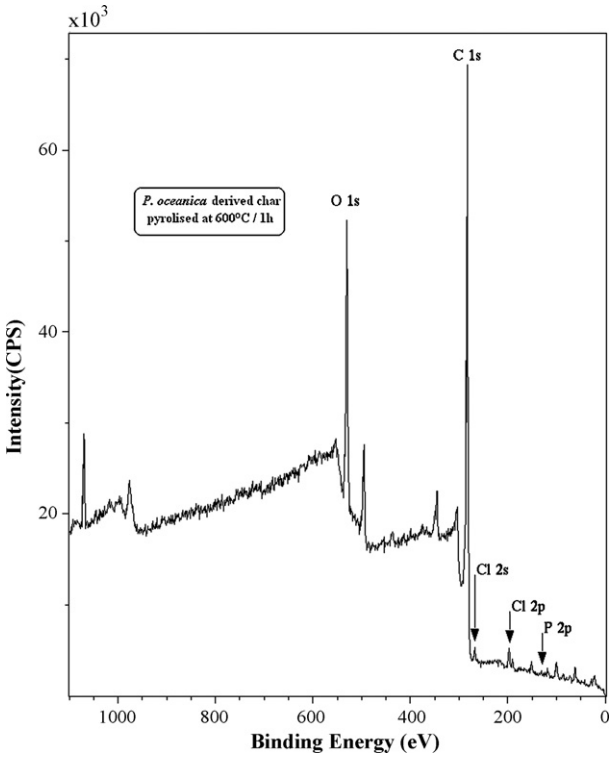

Fig. 7. XPS spectrum of *P. oceanica* derived chars pyrolysed at 600 °C for 1 h.

of micropores volume and a well-developed mesoporosity, which consolidate the previously mentioned assumption.

3.3.3. Elemental and textural characterisation

3.3.3.1. XPS spectroscopy. In order to investigate the variation of the elemental composition within the upper 10 nm of the char surface, the X-ray photoelectron spectrum (XPS) was recorded, in Fig. 7, for the case of a char sample (pyrolysed at 600 °C for 1 h, as the char contains equal amounts of graphite and disorder carbons). Indeed, XPS is one of the most interesting methods frequently used for non-destructive characterisation of coal surface [25].

The comparison based on the XPS analysis performed between the char sample and its precursor (raw fibres) revealed, in Table 3, that the pyrolysis tends to increase the carbon fraction toward the oxygen one, mainly due to the volatilisation of the oxygenated compounds.

3.3.3.2. Scanning electron microscopy. Fig. 8A–D shows the scanning electron microscope (SEM) images of the *P. oceanica* derived chars, produced under several pyrolysis temperatures. Compared to the precursor's SEM presented in Fig. 1B, the pyrolysed fibres start to generate a porous structure from the lowest investigated temperature (300 °C). Then, as the pyrolysis temperature increases, the fibrous char begins to show more pores in its inner structure, which agrees the assumption made after the weight loss increase revealed after the augmentation of the pyrolysis temperature (i.e.

Table 3
Percent composition of O (1s) and C (1s) and related O/C ratios for raw *P. oceanica* fibres and derived char pyrolysed at 600 °C for 1 h.

	O (1s)	C (1s)	O/C
Raw *P. oceanica* fibres	34.66%	42.10%	0.82
P. oceanica derived char (600 °C/1 h)	16.68%	66.01%	0.25

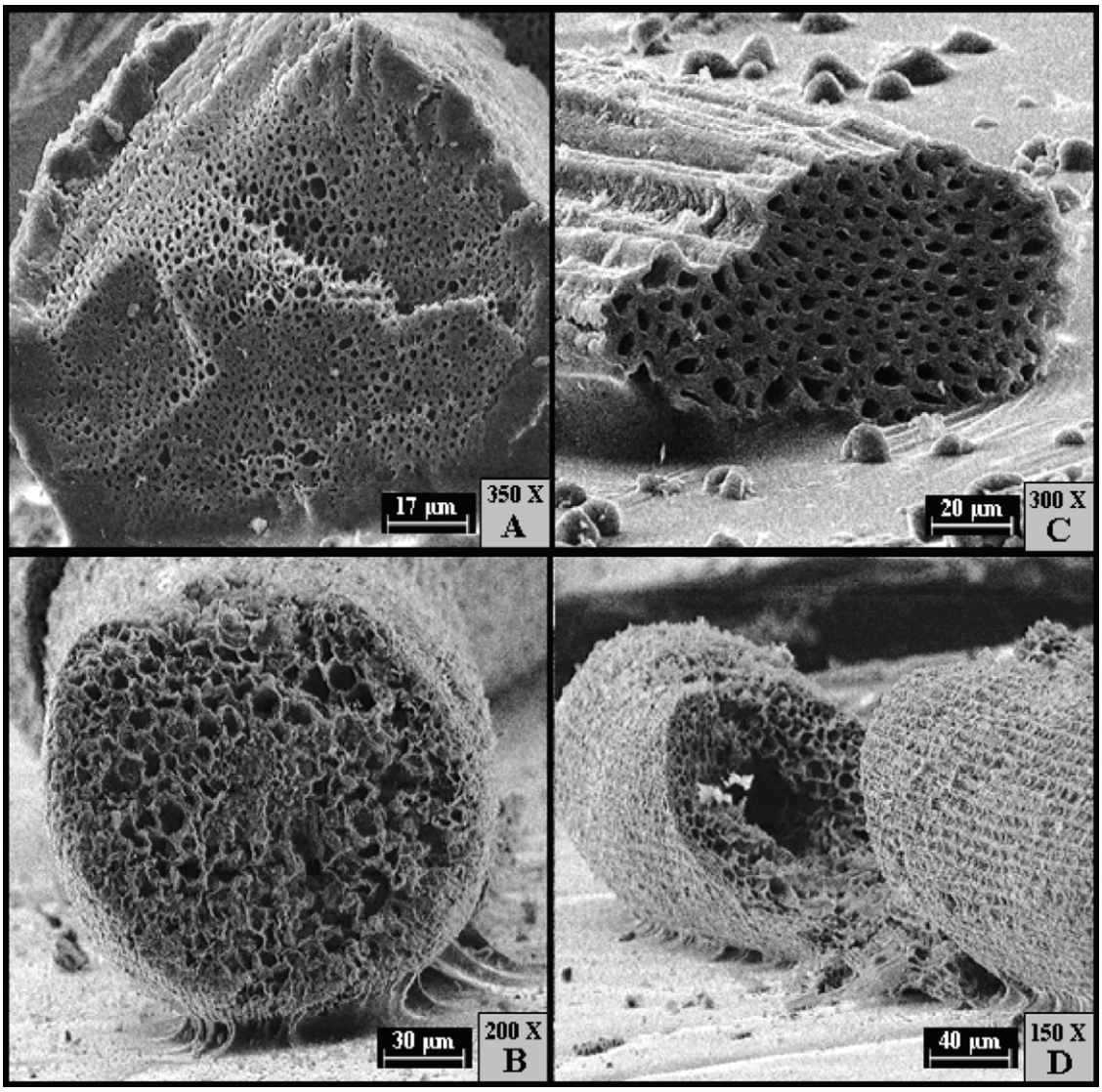

Fig. 8. SEM images of *P. oceanica* derived chars pyrolysed for 1 h at various temperatures: 300 °C (A), 400 °C (B), 700 °C (C) and 800 °C (D).

gasification of organic compounds) and previously verified via XPS analysis.

Besides, an interesting image (Fig. 9) was taken for the inner wall of a pore within the char produced at 600 °C for 1 h. It was revealed that the pyrolysis of the *P. oceanica* fibres would, in addition to the creation of pores, induce a kind of stripy texture in the inner walls, which definitely would enhance the overall surface area.

3.4. Physically activated carbons

3.4.1. Effect of activation time

The effect of the physical activation time on the evolution of the burn-off percentage is depicted in Fig. 10 for an exposure interval from 20 to 720 min. As shown, the activated carbon burn-off was seen to increase from 14.7 to 78.3% as activation period increased from 20 to 720 min. Such tendency is mainly explained by the increasing rate of reaction between carbon and water steam which leads to the enhancement of the volatilisation process. Indeed, the water steam had the ability to penetrate into the solid material and further helped in desorption, distillation and more efficient removal of the volatiles still remaining in the char [26]. It also helped in stabilising the radicals obtained during thermal decomposition, hence increasing the removal of volatile matter [27]. The same trend was also mentioned for the case of oil palm wood [28].

3.4.2. Porosity and surface area

From the eight previously produced PACs, four of them were analysed to monitor the effect of the physical activation on the evolution of both surface area and porous structure (20, 120, 300 and 720 min of activation, i.e. 14.7, 23.4, 31.7 and 78.8% of burn-off). The analyses of the nitrogen adsorption of the selected PACs activated carbons are shown in Fig. 11, the related BET and BJH calculations illustrated in Table 4 and the pore size distribution of the some PACs samples depicted in Fig. 6B.

Fig. 11 showed that an increase in the water steam activation time resulted in the production of activated carbons with nitrogen adsorption isotherms containing three characteristic regions: (i) the nitrogen uptake increased linearly at $P/P_0 < 0.01$; (ii) the first knee of the isotherms became more open at $0.01 < P/P_0 < 0.6–0.98$, depending on the activation time, and (iii) a second knee occurs above relative pressure 0.6–0.98.

Hence, based on the first part of the curves ($P/P_0 < 0.01$), associated to the plateau reached for relative pressures between 0.01 and 0.5 for all tested PACs, the shape resembles the type I of the BDDT

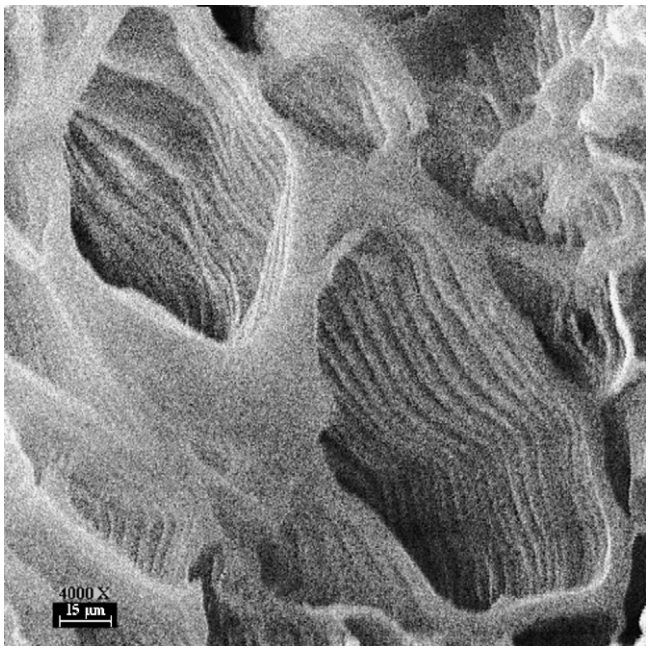

Fig. 9. SEM image of the internal pore structure of the char pyrolysed at 600 °C for 1 h.

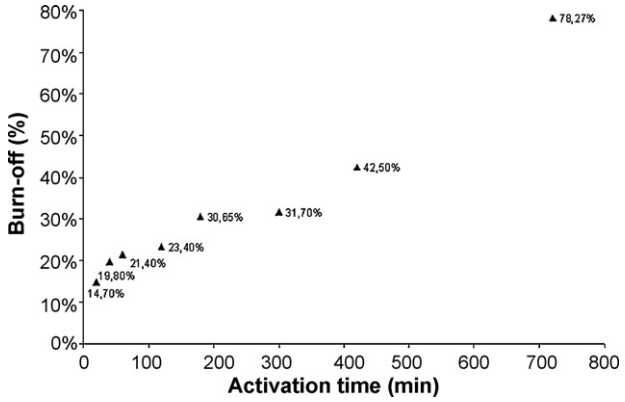

Fig. 10. Effect of the water steam activation time on the burn-off variation.

classification. Thus, it could be deduced that the physical activation was able to induce the creation of a microporosity in all PACs. Besides, the observed characteristics related to the second knee, indicated a significant development of the mesoporosity, which differs as the activation time is increased. Indeed, Fig. 10 indicated that increasing the water steam activation period affected the shape of the isotherms in the mesopore region, especially for the "PAC720" sample. As shown, all isotherms contain a second knee in the meso- and macropore region indicating the occurrence of the important process of pore widening.

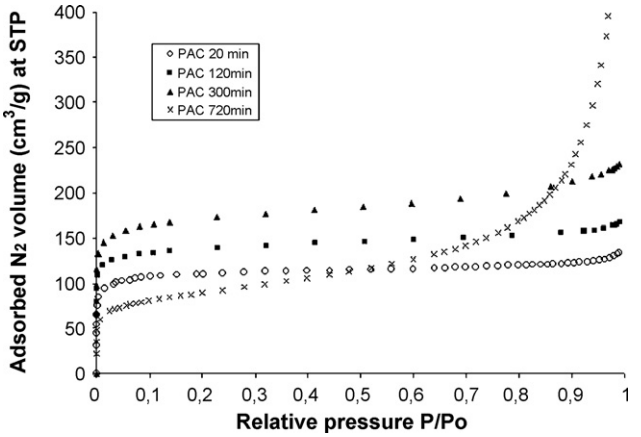

Fig. 11. Adsorption isotherm of nitrogen at 77 °K by physically activated carbons produced at 600 °C and under different activation times.

However, the position of this knee changes slightly for PAC20, 120 and 300 (i.e. the related relative pressures decrease from 0.98, 0.95 to 0.90, respectively). Such change in the shape of the N_2 isotherm is clearly illustrated in the case of PAC720. Indeed, the second knee starts at relative pressure of about 0.60. Besides, its overall isotherm shape tends to match the type IV curve, which is traditionally attributed to the mesoporous solids.

All those assumptions, based on the BET analysis, were in perfect agreement with the BJH analysis. Indeed, as shown in Table 4, the PACs (20, 120 and 300 min of activation) are mesoporous carbons with a significant fraction of micropores. For instance, the percent of mesoporosity of PAC20 is 64% with a microporosity of about 28%. Besides, it has to be mentioned that within that group, the increase of the activation time leads to the augmentation of the mesoporous fraction and the decrease of the microporous one. In that issue, from 20 to 300 min of activation, the mesopore percentage increases from 64 to 74% and the micropore fraction decreases from 28 to 13%. Thus, the mesoporosity seems to be developed from the micropores, which occurs during the physical activation gasification phase, resulting in loss of carbon. This loss of carbon results in pore widening and the development of mesoporosity.

On the other hand, the PAC 720, which shows a classical Type II shape, the major part of the induced porosity is mesoporous-type. Indeed, as illustrated in Table 4, 86% of the pores are mesopores with only 2% of micropores. The same tendency was also reported using ACs derived from biomass flax fibre waste [29], coconut shell and two commercial ACs [30].

3.4.3. Elemental and textural characterisation

3.4.3.1. XPS spectroscopy. The XPS analysis was used in order to evaluate the changes in the chemical bonding states and concentrations of the surface functional groups related to the increase of the activation time. According to the area-simulating curve, the percentage of each functional group was calculated

Table 4
Surface and porous texture parameters of physically activated carbons derived from *P. oceanica* fibres.

Activation time (min)	20	120	300	720
BET surface area (m^2/g)	375	496	615	313
Total pore volume (cm^3/g)	0.056	0.086	0.160	0.707
Micropore volume (cm^3/g) ($d < 2$ nm)	0.016 (28%)[a]	0.018 (21%)[a]	0.021 (13%)[a]	0.016 (2%)[a]
Mesopore volume (cm^3/g) (2 nm < d < 50 nm)	0.036 (64%)[a]	0.061 (71%)[a]	0.118 (74%)[a]	0.610 (86%)[a]
BJH average pore width (nm)	13.03	13.26	13.09	17.16
Bulk density (g/cm^3)	0.535	0.570	0.440	0.405

[a] Porosity percentage; d: pore diameter.

Table 5
Distribution of carbon and oxygen forms occurring on the AC surface from XPS data (at.%).

PAC sample	Peak from C1s spectrum binding energy (eV)					Peak from O1s spectrum binding energy (eV)		
	(I)	(II)	(III)	(IV)	(V)	(I′)	(II′)	(III′)
PAC60	43.51	24.39	20.49	6.12	5.49	40.72	20.35	38.93
PAC120	46.31	23.45	20.20	6.19	3.65	47.16	30.16	22.66
PAC180	51.51	19.29	19.16	5.91	4.13	45.99	24.55	29.46
P1C420	51.46	18.47	18.36	6.18	5.53	37.64	27.91	34.45

for some PACs are listed in Table 5, and the C1s and O1s spectra of a PAC sample (PAC300) are depicted in Fig. 12A and B, respectively.

Thus, it was shown that the C1s spectrum has been deconvoluted into five components with chemical shifts corresponding to: (I) graphite type (284.1–284.4 eV); (II) amorphous carbon, hydroxyl groups, phenolic, alcohol or ether aromatic carbon (284.8–285.2 eV); (III) carbonyl groups (285.5–286.1 eV); (IV) carboxyl and ester groups (286.3–287.6 eV) and (V) a peak corresponding to π–π^* transitions in the aromatic carbon (289.5–290.0 eV) [16,22]. The O1s spectrum was fitted to three components: (I′) C = O groups (530–531.6 eV); (II′) C–OH or C–O–C groups (532.7–533.3 eV) and (III') the last peak corresponding to chemisorbed oxygen (534.8–535.7 eV) [31].

According to the related results, the increase of the activation time leads to the enhancement of the graphite carbon amount. Indeed, from 60 to 420 min of exposure time, the percent atomic concentration increases from 43.5 to 51.5%. On the other hand, such activation time rising exerts an influence of the amorphous "disordered" carbon by diminishing their fraction, proportionally (i.e. 24.4% for PAC60 to 18.5% PAC420).

Dealing with the oxygen fraction, it was seen that the major oxygenated components are the C=O groups. Besides, it was also shown that the fraction of the C—OH or C—O—C groups increases from 20.3 to 27.9% as the activation time is increased from 60 to 420 min.

3.4.3.2. Scanning electron microscopy. The SEM images presented in Fig. 13, shows the evolution of the porous structure with respect to the activation time, for some samples of *P. oceanica* PACs. Thus, as the char is activated for longer periods, the pores begin to be more individualised and "clean". Indeed, after the pyrolysis phase, some of the pores might have been blocked by deposition of carbonaceous tar materials during the cooling period after pyrolysis. Thereafter, the water steam activation starts to remove this deposit, and as the time increases, the tar elimination will be enhanced as previously explained when the burn-off percent increased. Then, once all the tar is removed from the pores, it seems that the steam action starts to modify the pore morphology mainly by transforming the micropores onto mesopores, which is in agreement with the BJH analysis.

3.5. Comparison between the porous properties of P. oceanica derived carbonaceous materials and those prepared from other bioresources

Both *P. oceanica* derived char and PAC were compared with those produced from other biological precursors, in order to situate the

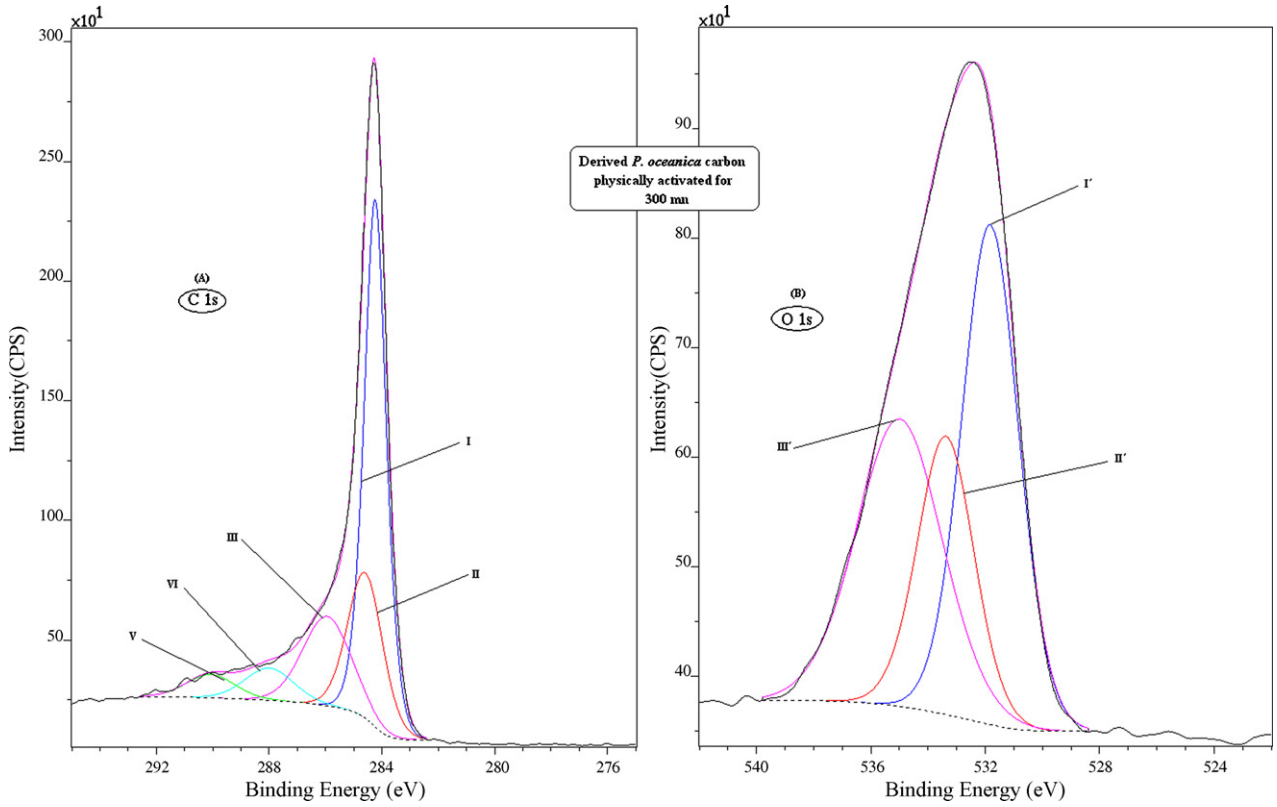

Fig. 12. XPS spectrum analysis on C1s (A) and O1s (B) apices of physically activated carbon produced at 600 °C for 300 min.

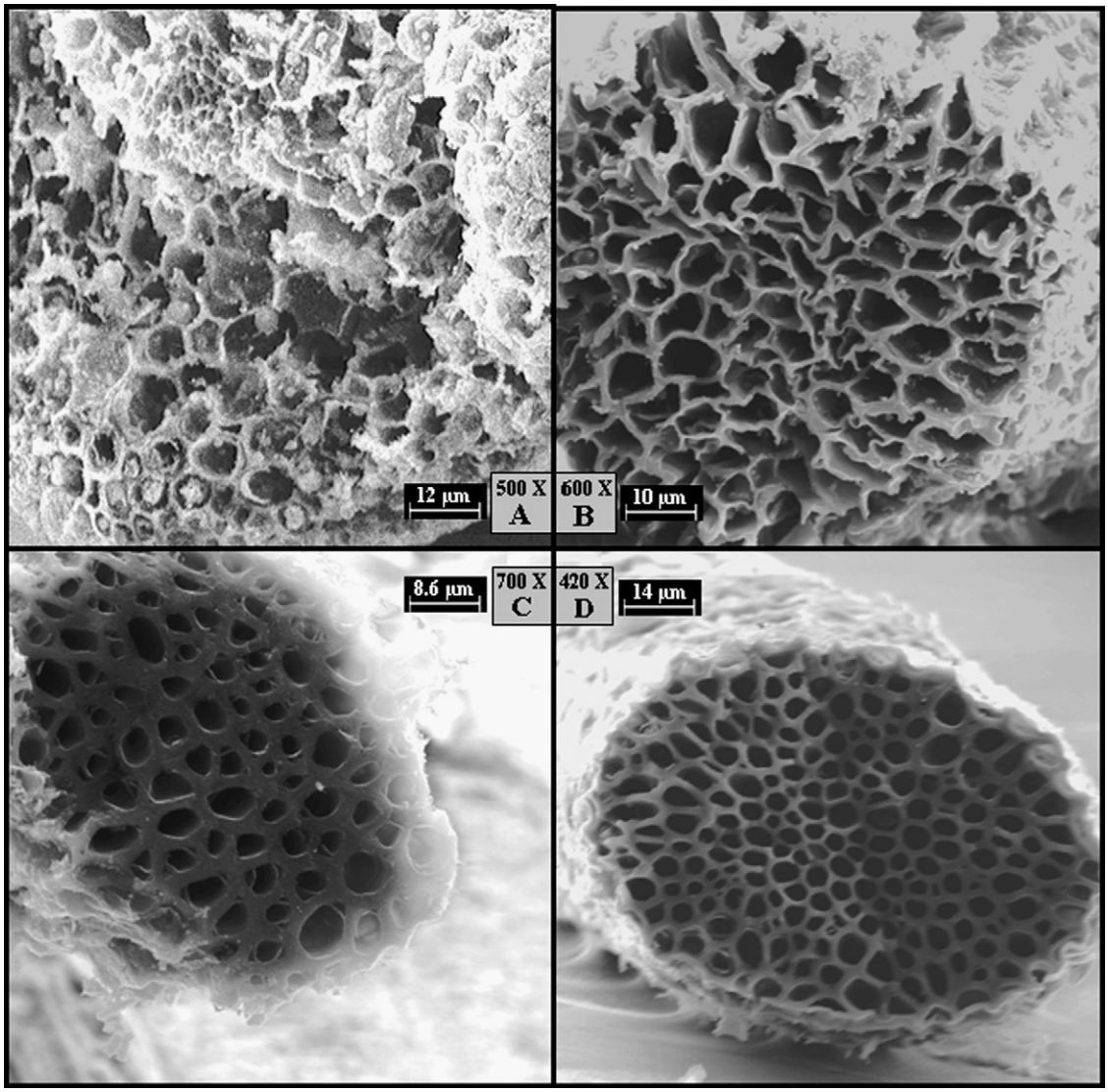

Fig. 13. SEM images of *P. oceanica* derived carbons physically activated at various times: 20 min (A), 120 min (B), 300 min (C) and 720 min (D).

Table 6
Comparison of surface and porous texture parameters of pyrolyzed chars derived from *P. oceanica* fibres and other bioressources.

Pyrolyzed chars derived from:	BET surface (m^2/g)	V_{micro} (cm^3/g)	V_{meso} (cm^3/g)	Average pore width (nm)	References
P. oceanica fibres (600 °C/1 h)	111	0.004	0.028	16.99	This study
Date stones (600 °C/1 h)	50	0.20	NA	NA	[32]
Chicken manure (600 °C/5 h)	4	< 0.01	NA	8.8	[25]
Jute fibres (950 °C/2 h)	2	0	0	NA	[34]
Coconut fibres (950 °C/2 h)	1	0	0	NA	[34]

NA: not available.

Table 7
Comparison of surface and porous texture parameters of physically activated carbons derived from *P. oceanica* fibres and other bioressources.

Physically activated carbons derived from:	BET surface (m^2/g)	V_{micro} (cm^3/g)	V_{meso} (cm^3/g)	Average pore width (nm)	References
P. oceanica fibres (600 °C/5h)	615	0.021	0.118	13.09	This study
Date stones (600 °C/6 h)	514	0.673	NA	NA	[32]
Vetiver roots (820 °C/4 h)	576	0.220	0.090	1.35	[3]
Eucalyptus wood (880 °C/2.5 h)	1042	0.393	NA	NA	[33]
Rice husk (880 °C/2.5 h)	194	0.072	NA	NA	[33]
Chicken manure (800 °C/0.5 h)	788	0.290	NA	2.02	[25]
Jute fibres (950 °C/0.5 h)	657	0.289	0.070	NA	[34]
Coconut fibres (950 °C/0.5 h)	534	0.238	0.013	NA	[34]
Sugarcane bagasse (900 °C/5 h)	860	0.460	NA	0.60	[35]

NA: not available.

use of this marine fibre to produce carbonaceous adsorbents. Such comparison is based ion the surface area and the generated porous structure.

Dealing with chars, Table 6 shows that the pyrolysis of *P. oceanica* fibres, without any further activation, is able to induce a porous structure. At this stage, other bioresources are unable to do so (i.e. case of jute and coconut fibre [34]). For the other precursors, which are able to create pores after the pyrolysis step, the *P. oceanica* derived char are characterised by both major mesoporous structure and relatively high inner surface (*cf.* Table 6).

On the other, a comparative study on both surface area and porous properties was realised between *P. oceanica* derived PACs and those prepared from other biomaterials. Results of this comparison are illustrated in Table 7. As shown, the physical activation of *P. oceanica* fibres produces PAC with a surface area of about 615 m^2/g, which is an average value compared to the compared PAC samples. However, the main characteristic of the posidonia PAC is the well-developed mesopores with an average pore width of 13.1 nm.

4. Conclusions

In this research, renewable, highly available and low cost *Posidonia oceanica* marine fibres were investigated as precursor for pyrolysed and physically activated carbons preparation. The characterisation of the raw biomass showed that the major component was holocellulose (almost 60% of the dry weight) with 27% of lignin. Then, based on the XPS, BET, BJH and SEM analysis, the results revealed that the pyrolysis starts to generate the porous structure and the water steam activation enhance the pore creation process. Indeed, starting from a BET surface of about 111 m^2/g for a char sample (pyrolysed at 600 °C for 1 h) the physical activation tends to enhance the development of the porous structure and thereafter increase the overall surface area, which reaches its high value (615 m^2/g) after 300 min of activation. Once the activation time is increased further (720 min), the BET surface decreases to 313 m^2/g. Such phenomenon could be related to the eventual collapse of some pore walls in the core of the fibre. Besides, the BJH analysis revealed that most of the *P. oceanica* derived PACs had an inner mesoporous morphology.

Acknowledgements

This research was supported by the International Foundation for Science, Stockholm, Sweden, and the Organisation for the Prohibition of Chemical Weapons, The Hague, The Netherlands, through a grant to Dr. Mohamed Chaker Ncibi. The first author also gratefully acknowledges the AUF (Agence Universitaire de la Francophonie) for the 2006/2007 and 2007/2008 doctoral fellowships.

References

[1] A. Ouensanga, L. Largitte, M.A. Arsene, The dependence of char yield on the amounts of components in precursors for pyrolysed tropical fruit stones and seeds, Micropor. Mesopor. Mater. 59 (2003) 85–91.
[2] M.L. Sanchez, A.M. Garcia, M.A. Diez, E.M. Correa, J. Gomez, A.N. Gisbert, Preparation of activated carbons previously treated with hydrogen peroxide: study of their porous texture, Appl. Surf. Sci. 252 (2006) 5984–5987.
[3] S. Gaspard, S. Altenor, E.A. Dawson, P.A. Barnes, A. Ouensanga, Activated carbon from vetiver roots: gas and liquid adsorption studies, J. Hazard. Mater. 144 (2007) 73–80.
[4] B.S. Girgis, M.F. Ishak, Activated carbon from cotton stalks by impregnation with phosphoric acid, Mater. Lett. 39 (1999) 107–114.
[5] C. Ng, J.N. Losso, W.E. Marshall, R.M. Rao, Physical and chemical properties of selected agricultural by-products based activated carbons and their ability to adsorb geosim, Bioresour. Technol. 84 (2000) 177–185.
[6] G. Bello, R. Garcia, R. Arriagada, A. Sepulveda-Escribano, F. Rodriguez-Reinoso, Carbon molecular sieves from *Eucalyptus globulus* charcoal, Micropor. Mesopor. Mater. 56 (2002) 139–145.
[7] F. Banat, S. Al-Asheh, L. Al-Makhadmeh, Evaluation of the use of raw and activated date pits as potential adsorbents for dye containing waters, Process Biochem. 39 (2003) 192–202.
[8] A. Aygun, S.Y. Karakas, I. Duman, Production of granular activated carbon from fruit stones and nutshells and evaluation of their physical, chemical and adsorption properties, Micropor. Mesopor. Mater. 66 (2003) 189–195.
[9] B.H. Hameed, A.T. Din, A.L. Ahmad, Adsorption of methylene blue onto bamboo-based activated carbon: kinetics and equilibrium studies, J. Hazard. Mater. 141 (2007) 819–825.
[10] J.A. Menéndez-Diaz, I. Martin-Gullon, Types of carbon adsorbents and their production, in activated carbon surfaces in environmental remediation, in: Teresa, J. Bandosz (Eds.), Interface Science and technology, Vol. 7, Academic Press, Elsevier, 2006.
[11] A. Ouensanga, Variation of fiber composition in sugarcane stalks, Wood Fiber Sci. 21 (1989) 105–111.
[12] E.W. Crampton, L.A. Maynard, The relation of cellulose and lignin content to the nutritive value animal feeds, J. Nutr. 15 (1938) 383–395.
[13] E.P. Barret, P.B. Joyner, P. Halenda, The determination of pore volume and area distribution in porous substances. I. Computations from nitrogen isotherms, J. Am. Chem. Soc. 73 (1951) 373–380.
[14] S.J. Gregg, K.S. Sing, Adsorption, Surface Area and Porosity, Academic Press, 1982.
[15] C.J. Valle, M.G. Corza, J.P. Villegas, V.G. Serrano, Study of cherry stones as raw material in preparation of carbonaceous adsorbents, J. Anal. Appl. Pyrol. 73 (2005) 59–67.
[16] G.G. Stavropoulos, A.A. Zabaniotou, Production and characterization of activated carbons from olive-seed waste residue, Micropor. Mesopor. Mater. 82 (2005) 79–85.
[17] D.M. Mackay, P.V. Roberts, The dependence of char and carbon yield on lignocellulosic precursor composition, Carbon 20 (1982) 87–94.
[18] A. Bacaoui, A. Yaacoubi, A. Dahbi, C. Bennouna, R.P. Luu, F.J. Hodar, J.R. Utrilla, C.M. Castilla, Optimization of conditions for the preparation of activated carbons from olive-waste cakes, Carbon 39 (2001) 425–432.
[19] E. Jakab, O. Faix, F. Till, T. Székely, Thermogravimetry/mass spectrometry study of six lignins within the scope of an international round robin test, J. Anal. Appl. Pyrolysis 35 (1995) 167–179.
[20] S. Ouajai, R.A. Shanks, Composition, structure and thermal degradation of hemp cellulose after chemical treatments, Polym. Degrad. Stabil. 89 (2005) 327–335.
[21] G. Várhegyi, M.J. Antal Jr., E. Jakab, P. Szabó, Kinetic modelling of biomass pyrolysis, J. Anal. Appl. Pyrolysis 42 (1997) 73–87.
[22] J.A. Caballero, A. Marcilla, J.A. Conesa, Thermogravimetric analysis of olive stones with sulphuric acid treatment, J. Anal. Appl. Pyrolysis 44 (1997) 75–88.
[23] J.P. Boudou, P. Parent, F.S. Garcia, S.V. Rodil, A.M. Alonso, J.M. Tascon, Nitrogen in aramid-based activated carbon fibers by TPD, XPS and XANES, Carbon 44 (2006) 2452–2462.
[24] S. Brunauer, L.S. Deming, W.S. Deming, E. Teller, On a Theory of the van der Waals adsorption of gases, J. Am. Chem. Soc. 62 (1940) 1723–1732.
[25] S. Koutcheiko, C.M. Monreal, H. Kodama, T. McCracken, L. Kotlyar, Preparation and characterization of activated carbon derived from the thermo-chemical conversion of chicken manure, Biores. Technol. 98 (2007) 2459–2464.
[26] A.C. Lua, J. Guo, Preparation and characterization of activated carbons from oil-palm stones for gas-phase adsorption, Colloids Surf. A: Physicochem. Eng. Aspects 179 (2001) 151–162.
[27] V. Minkova, M. Razvigorova, E. Bjornbom, R. Zanzi, T. Budinova, N. Petrov, Effect of water vapour and biomass nature on the yield and quality of the pyrolysis products from biomass, Fuel Process. Technol. 70 (2001) 53–61.
[28] A.L. Ahmad, M.M. Loh, J.A. Aziz, Preparation and characterization of activated carbon from oil palm wood and its evaluation on methylene blue adsorption, Dyes Pigm. 75 (2007) 263–272.
[29] P.T. Williams, A.R. Reed, Development of activated carbon pore structure via physical and chemical activation of biomass fibre waste, Biomass Bioenergy 30 (2006) 144–152.
[30] E.M. Correa, M.A. Diez, A.M. Garcia, J.G. Gomez, Determination of the fractal dimension of activated carbons: Two alternative methods, Appl. Surf. Sci. 252 (2006) 6102–6105.
[31] S. Figaro, S. Louisy-Louis, J. Lambert, J.J. Ehrhardt, A. Ouensanga, S. Gaspard, Adsorption studies of recalcitrant compounds of molasses spentwash on activated carbons, Water Res. 40 (2006) 3456–3466.
[32] C. Bouchelta, M.S. Medjram, O. Bertrand, J.-P. Bellat, Preparation and characterization of activated carbon from date stones by physical activation with steam, J. Anal. Appl. Pyrolysis 82 (1) (2008) 70–77.
[33] A. Amaya, N. Medero, N. Tancredi, H. Silva, C. Deiana, Activated carbon briquettes from biomass materials, Bioresour. Technol. 98 (2007) 1635–1641.
[34] N.H. Phan, S. Rio, C. Faur, L. Le Coq, P. Le Cloirec, T.H. Nguyen, Production of fibrous activated carbons from natural cellulose (jute, coconut) fibers for water treatment applications, Carbon 44 (2006) 2569–2577.
[35] M. Valix, W.H. Cheung, G. McKay, Preparation of activated carbon using low temperature carbonisation and physical activation of high ash raw bagasse for acid dye adsorption, Chemosphere 56 (2004) 493–501.